

Stellar Feedback & Bulge Formation in Clumpy Disks

Philip F. Hopkins^{1*}, Dusan Kereš^{1,2}, Norman Murray^{3,4},
Eliot Quataert¹, & Lars Hernquist⁵

¹*Department of Astronomy and Theoretical Astrophysics Center, University of California Berkeley, Berkeley, CA 94720*

²*Hubble Fellow*

³*Canadian Institute for Theoretical Astrophysics, 60 St. George Street, University of Toronto, ON M5S 3H8, Canada*

⁴*Canada Research Chair in Astrophysics*

⁵*Harvard-Smithsonian Center for Astrophysics, 60 Garden Street, Cambridge, MA 02138, USA*

Submitted to MNRAS, November, 2011

ABSTRACT

We use numerical simulations of isolated galaxies to study the effects of stellar feedback on the formation and evolution of giant star-forming gas “clumps” in high-redshift, gas-rich galaxies. Such galactic disks are unstable to the formation of bound gas-rich clumps whose properties initially depend only on global disk properties, not the microphysics of feedback. In simulations without stellar feedback, clumps turn an order-unity fraction of their mass into stars and sink to the center, forming a large bulge and kicking most of the stars out into a much more extended stellar envelope. By contrast, strong radiative stellar feedback disrupts even the most massive clumps after they turn $\sim 10 - 20\%$ of their mass into stars, in a timescale of $\sim 10 - 100$ Myr, ejecting some material into a super-wind and recycling the rest of the gas into the diffuse ISM. This suppresses the bulge formation rate by direct “clump coalescence” by a factor of several. However, the galactic disks do undergo significant internal evolution in the absence of mergers: clumps form and disrupt continuously and torque gas to the galactic center. The resulting evolution is qualitatively similar to bar/spiral evolution in simulations with a more homogeneous ISM.

Key words: galaxies: formation — galaxies: evolution — galaxies: active — star formation: general — cosmology: theory

1 INTRODUCTION

In recent years, considerable attention has been paid to what appears to be a population of massive ($M_* \sim 10^{10} - 10^{11} M_\odot$), gas-rich ($M_{\text{gas}}/(M_{\text{gas}} + M_*) \sim 0.3 - 0.7$), rapidly star forming ($\dot{M}_* \sim 10 - 200 M_\odot \text{ yr}^{-1}$) “disk” galaxies (flattened and apparently rotationally supported, albeit with the ratio of rotational to random velocity $V/\sigma \sim \text{a few}$) at redshifts $z \sim 2 - 3$ (see e.g. Chapman et al. 2005; Greve et al. 2005; Tacconi et al. 2006; Genzel et al. 2008; Tacconi et al. 2010; Shapiro et al. 2009; Daddi et al. 2010; Förster Schreiber et al. 2006, 2011b). The most extreme star-forming populations at these redshifts (with $\dot{M}_* \sim 100 - 3000 M_\odot \text{ yr}^{-1}$) appear to be major merger-induced starbursts, but these “disky” systems dominate the intermediate-luminosity population which includes a large fraction of the total SFR density (see references above and Tacconi et al. 2008). The morphology of the young stars (observed in the rest-frame UV and optical light) and star-forming or molecular gas (e.g. $\text{H}\alpha$) is characteristically irregular (“clumpy” or “clump-chain” morphologies), with a significant fraction (tens of percent) of the light in $\sim \text{a few}$ massive ($\gg 10^8 M_\odot$), $\sim \text{kpc}$ -scale clumps or blobs (Griffiths et al. 1994; Cowie et al. 1995; Gialalisco et al. 1996; Abraham et al. 1996; Elmegreen et al. 2004b,a, 2005b; Kriek et al. 2009; Genzel et al. 2011; Swinbank et al. 2011).

Theoretically, the origin of these morphologies is controversial. Some early models argued they were irregular because of ongoing mergers (Somerville et al. 2001); observations of local analogues (and studies in which these systems are mock-observed as if they were at high redshifts) suggest that this is true for least some fraction of the observed systems (Overzier et al. 2010, 2009; Petty

et al. 2009). However, the constraints on the structure and kinematics of the massive $z \sim 2$ systems suggest that a sizeable fraction are more quiescent¹ (Shapiro et al. 2008; Förster Schreiber et al. 2006, 2011a), although this is not definitive evidence against mergers (Robertson & Bullock 2008; Hammer et al. 2009). And the merger rate may not be sufficiently high to explain the abundance of these intermediate-SFR systems (e.g. Dekel et al. 2009b; Stewart et al. 2009; Hopkins et al. 2010; Hopkins & Hernquist 2010).

An alternative explanation for the observed morphologies is that clumpiness stems from disk fragmentation. Any gas disk in which cooling is efficient (cooling time less than the dynamical time so that turbulent support dissipates in a crossing time, which is easily satisfied here) will fragment at the Toomre scale, $R_T \sim \sigma^2/\pi G \Sigma$ or $M_T \sim \sigma^4/\pi G^2 \Sigma$ (Toomre 1964); for disks which equilibrate at marginal stability (Toomre $Q \sim 1$), this is just $R_T \sim f_{\text{gas}} R_{\text{disk}}$ ($M_T \sim f_{\text{gas}}^3 M_{\text{disk}}$).² In the Milky Way, these clumps correspond to massive GMCs ($R \sim 100 \text{ pc}$, $M \sim 10^6 M_\odot$). But in a massive, gas-rich disk, the scale-length and mass of the resulting clumps can be as large as $\sim \text{kpc}$ and $\sim 10^8 - 10^9 M_\odot$, respectively, similar to the structures observed.

This instability has been well-known for ~ 40 years. The implications of such clumping in the ISM are less clear, however. If there were no feedback from stars to expel mass from GMCs/clumps, they would (locally) collapse in a few free-fall

¹ By “quiescent” here, we mean non-interacting/non-merging, as opposed to “quenched” or non-star forming.

² We have dropped numerical pre-factors that depend on the detailed disk structure. Also we could take f_{cold} instead of f_{gas} to reflect the dynamically thin/cold stellar components, although in detail the scaling for a gas plus stellar system, while qualitatively similar, becomes much more complex.

* Einstein Fellow. E-mail: phopkins@astro.berkeley.edu

times and turn most of their mass into stars. They would then sink to the galaxy center under the influence of dynamical friction on a timescale $t_{\text{sink}} \sim t_{\text{orbit}} M_{\text{disk}}/M_T$; for GMCs, this would take a Hubble time, but for massive clumps in the high redshift systems of interest, this could occur in a few disk orbital periods ($\sim 30 - 60$ clump dynamical times, or ~ 0.5 Gyr). This sinking would quickly build up a \sim kpc-scale bulge (Shlosman & Noguchi 1993; Noguchi 1999). This is also well-known and has been seen since the first simulations of very gas-rich disks (Hernquist 1989; Barnes & Hernquist 1991; Shlosman & Noguchi 1993; Barnes & Hernquist 1996; Sommer-Larsen et al. 1999; Robertson et al. 2004).

However, in the MW and nearby galaxies, typical GMCs are disrupted by stellar feedback after a few clump dynamical times (a few Myr), and recycle $\sim 95\%$ of their mass back into the ISM (Zuckerman & Evans 1974; Williams & McKee 1997; Evans 1999; Evans et al. 2009). This appears to be true for both low and high mass clouds, including local examples with masses and sizes very similar to those observed at high redshifts ($M_{\text{cloud}} \sim 10^8 - 10^9 M_{\odot}$; Wilson et al. 2003, 2006, and references therein).

If Toomre mass clumps were dispersed after a few dynamical times, it may be more accurate, in simulations, to treat the ISM as a “smooth” medium (i.e. not resolve the formation of individual clumps) rather than resolve clump formation but *not* their destruction/recycling. In fact, the one-way fragmentation seen in simulations without feedback was one of the primary motivations for modelers to include stronger prescriptions for stellar feedback in numerical galaxy models. Lacking the ability to explicitly resolve the processes that destroy clouds, this commonly amounted to assigning the gas a much larger “effective pressure” than its nominal thermal pressure so that runaway collapse could not occur. Such an effective pressure was intended to mimic a *global* average turbulent pressure maintained by a sub-grid process of continuous clump formation and destruction (Hernquist 1989; Springel & Hernquist 2003). This was also motivated by cosmological simulations – the one-way break-up of gas-rich disks was a significant factor preventing the formation of realistic disk galaxies and led to simulations which uniformly predicted bulge-to-disk ratios significantly larger than observed (Sommer-Larsen et al. 1999; Robertson et al. 2004; Governato et al. 2004, 2007). With the recent observations of these “clumpy” high-redshift galaxies, however, renewed interest has been paid to “weak feedback” models of the ISM (Immeli et al. 2004; Bournaud et al. 2007; Bournaud et al. 2008; Elmegreen et al. 2008; Agertz et al. 2009; Dekel et al. 2009a; Ceverino et al. 2010).

Without an *a priori* resolved model of stellar feedback, the dominant feedback physics and their effects remain uncertain. Genel et al. (2012) considered the evolution of gas-rich disks including various phenomenological models in which stellar feedback was parameterized by a “wind efficiency” (in short, for every mass ΔM_* in stars formed, a mass $\eta \Delta M_*$ is automatically kicked out of the galaxy). They showed that for order-unity wind efficiencies of the sort needed in cosmological models to explain the shape of the galaxy mass function (Oppenheimer et al. 2010), clumps form but are disrupted by feedback before turning a large fraction of their mass into stars and so do not spiral to the center. Observations have now suggested comparable wind mass-loading factors in the clumps (Genzel et al. 2011; Newman et al. 2012). These models, while a powerful “proof of concept,” are not able to *predict* the wind properties or detailed ISM structure. The studies of clumpy disks that have included physically-motivated models of stellar feedback have focused only on thermal heating from SNe; however, at the high gas densities of typical “clumps” ($\gtrsim 100 \text{ cm}^{-3}$)

gas which is shock-heated by SNe ejecta will cool in a timescale > 100 times shorter than its dynamical time, so these models unsurprisingly find similar results (in terms of clump survival) to feedback-free cases (Elmegreen et al. 2008; Ceverino et al. 2010). And at higher densities, in fact, the SNe timescale becomes longer than the local collapse/free fall time, so they cannot act efficiently (Evans et al. 2009).

A large number of feedback mechanisms may drive turbulence in the ISM and help disrupt GMCs, including: photo-ionization, stellar winds, radiation pressure from UV and IR photons, proto-stellar jets, cosmic rays, supernovae, and gravitational cascades from large scales (e.g. Mac Low & Klessen 2004, and references therein). In Hopkins et al. (2011) (Paper I) and Hopkins et al. (2012b) (Paper II) we developed a new set of numerical models to incorporate feedback on small scales in GMCs and star-forming regions, in simulations with pc-scale resolution.³ These simulations include the momentum imparted locally (on sub-GMC scales) from stellar radiation pressure, radiation pressure on larger scales via the light that escapes star-forming regions, HII photoionization heating, as well as the heating, momentum deposition, and mass loss by SNe (Type-I and Type-II) and stellar winds (O star and AGB). The feedback is tied to the young stars, with the energetics and time-dependence taken directly from stellar evolution models. Our models also include realistic cooling to temperatures < 100 K, and a treatment of the molecular/atomic transition in gas and its effect on star formation. We showed in Papers I & II that these feedback mechanisms produce a quasi-steady ISM in which giant molecular clouds form and disperse rapidly, after turning just a few percent of their mass into stars. This leads to an ISM with phase structure, turbulent velocity dispersions, scale heights, and GMC properties (mass functions, sizes, scaling laws) in reasonable agreement with observations. In Hopkins et al. (2012a) (Paper III), we showed that these same models of stellar feedback produce the elusive winds invoked in almost all galaxy formation models; the combination of multiple feedback mechanisms give rise to massive, multi-phase winds having a broad distribution of velocities, with material both stirred in local fountains and unbound from the disk.

In this paper, we use these models to study massive, GMC-analogue clumps in high-redshift star-forming disks, and their implications for bulge formation.

2 THE SIMULATIONS

The simulations used here are described in detail in Paper I (Sec. 2 & Tables 1-3) and Paper II (Sec. 2). We briefly summarize the most important properties here. The simulations were performed with the parallel TreeSPH code GADGET-3 (Springel 2005). They include stars, dark matter, and gas, with cooling, star formation, and stellar feedback.

Gas follows an atomic cooling curve with additional fine-structure cooling to < 100 K, with no “cooling floor” imposed. Star formation is allowed only in dense regions above $n > 1000 \text{ cm}^{-3}$, at a rate $\dot{\rho}_* = \epsilon \rho_{\text{mol}}/t_{\text{ff}}$ where t_{ff} is the free-fall time, $\rho_{\text{mol}} = f_{\text{H}_2} \rho$ is the molecular gas density, and $\epsilon = 1.5\%$ is the observed efficiency at these densities (Krumholz & Tan 2007). We follow Krumholz & Gnedin (2011) to calculate the molecular fraction f_{H_2} in dense gas as a function of local column density and metallicity. In Paper I and Paper II we show that the galaxy structure and SFR are basically

³ Movies of these simulations are available at <https://www.cfa.harvard.edu/~phopkins/Site/Research.html>

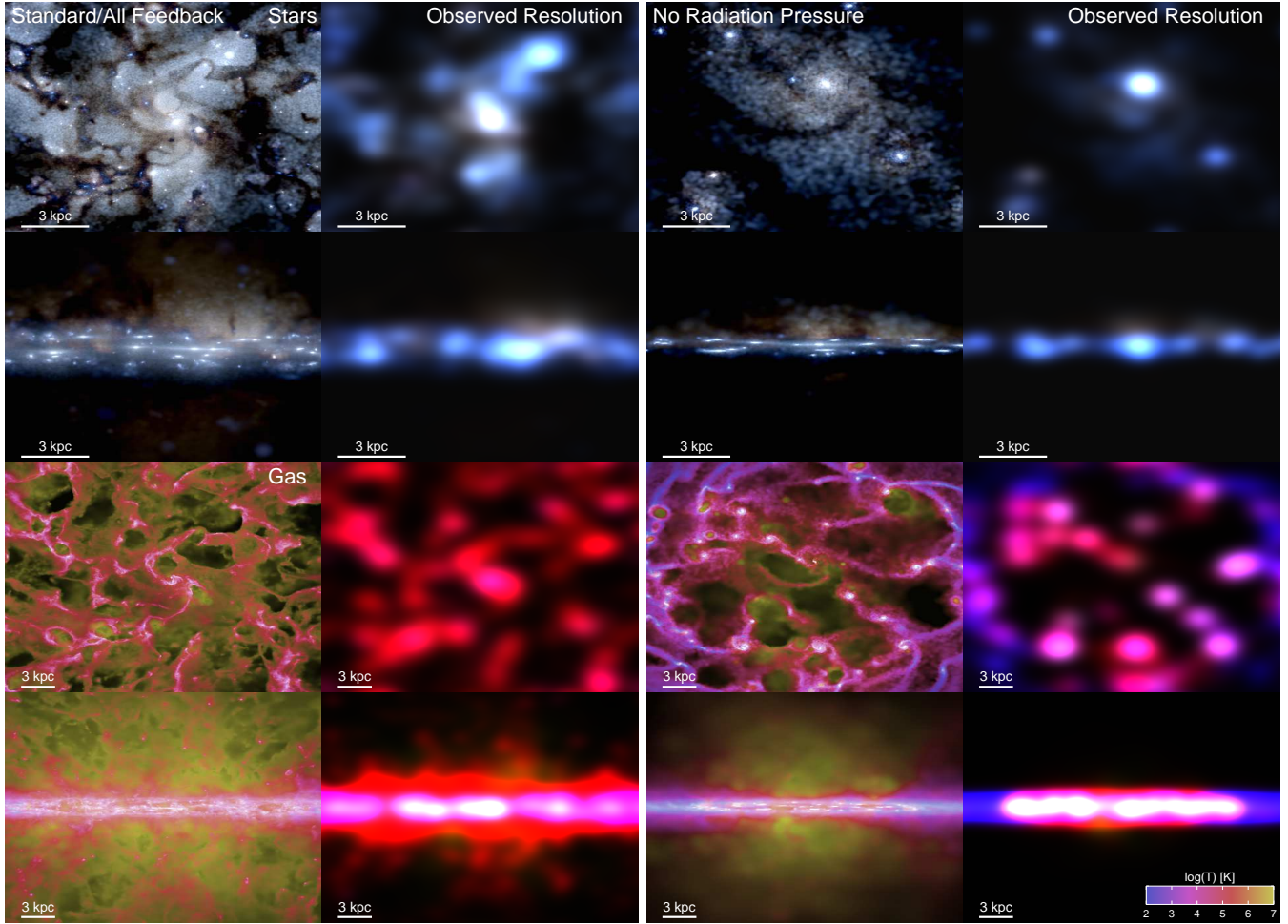


Figure 1. Morphology of the gas and stars in a simulation of a massive $z \sim 2-4$ rapidly star-forming disk with $\dot{M}_* \sim 100 M_\odot \text{ yr}^{-1}$. Images are shown at ~ 2 orbital times when the disk is in a feedback-regulated steady-state. We show face-on (upper) and edge-on (lower) projections. We compare two simulations: our “standard” model with all feedback mechanisms enabled (*left* two columns), and a model with identical conditions but radiation pressure (the dominant feedback mechanism) disabled (*right* two columns). *Top*: Stars. The image is a mock *ugr* (SDSS-band) composite, with the spectrum of all stars calculated from their known age and metallicity, and dust extinction/reddening accounted for from the line-of-sight dust mass.⁴ For each model, the *left* column is an image with effectively infinite resolution and depth (brightness follows a logarithmic scale with a stretch of ≈ 3 dex); the *right* column is the same image, convolved with a Gaussian PSF typical of HST WFC3 observations (FWHM $1.4 \text{ kpc} = 0.16''$ at $z = 2$) and with a linear stretch. *Bottom*: Gas. Brightness encodes projected gas density; color encodes gas temperature with blue/white being $T \lesssim 1000 \text{ K}$ molecular gas, pink $\sim 10^4 - 10^5 \text{ K}$ warm ionized gas, and yellow $\gtrsim 10^6 \text{ K}$ hot gas. Again, *left* is at extremely high resolution/depth (logarithmically scaled with a ≈ 6 dex stretch from $\sim 10^{-1} - 10^5 M_\odot \text{ pc}^{-2}$); *right* is the same with PSF convolution typical of e.g. SINFONI AO (FWHM $1.7 \text{ kpc} = 0.2''$ at $z = 2$) and linear stretch. Gravitational collapse forms massive kpc-scale star cluster complexes that give rise to the clumpy morphology (edge on, similar to “clump-chain” galaxies) that is further enhanced in the optical by patchy extinction. The clumps have considerable sub-structure. With all feedback included, strong outflows are present, emerging both from the complexes and the disk as a whole, driven by the massive star formation rate. These outflows maintain a thick gas disk and disrupt many of the clumps, which continuously re-form. With radiation pressure disabled, the outflows are much weaker (some “venting” hot gas), the clumps collapse further, are more clearly rotationally supported, and leave less of a diffuse low-brightness stellar background (having coalesced more efficiently).

independent of the small-scale SF law, density threshold (provided it is high), and treatment of molecular chemistry.

We consider an initial galaxy model intended to represent an (intentionally extreme) high-redshift massive “starburst disk” (typical of high-luminosity BzK galaxies or low-luminosity SMGs – intermediate SFR systems – at $z \sim 2-4$). The disk has a small ($B/T < 0.05$) initial Hernquist (1990) profile bulge ($M_b = 5 \times 10^9 M_\odot$ (chosen to be small to avoid suppressing disk instabilities and clearly isolate new bulge growth), scale-length $a = 1.2 \text{ kpc}$), an exponential stellar disk ($M_d = 3 \times 10^{10} M_\odot$; $r_d = 1.6 \text{ kpc}$ with sech² profile scale-height $h = 130 \text{ pc}$) a gas disk ($M_g = 7 \times 10^{10} M_\odot$; $r_g = 3.2 \text{ kpc}$), and a dark matter halo ($M_{\text{halo}} = 1.4 \times 10^{12} M_\odot$, con-

centration $c = 3.5$, scaled to lie on the mass-concentration relation for $z = 2$ halos). The model has $\approx 10^8$ total particles and 5 pc gravitational softening.

Stellar feedback is included, via a variety of mechanisms.

(1) **Local Momentum Flux** from Radiation Pressure, Supernovae, & Stellar Winds: Gas within a GMC (identified with an on-the-fly friends-of-friends algorithm) receives a direct momentum flux from the stars in that cluster/clump. The momentum flux is $\dot{P} = \dot{P}_{\text{SNe}} + \dot{P}_w + \dot{P}_{\text{rad}}$, where the separate terms represent the direct momentum flux of SNe ejecta, stellar winds, and radiation pressure. The first two are directly tabulated for a single stellar population as a function of age and metallicity Z and the flux is directed

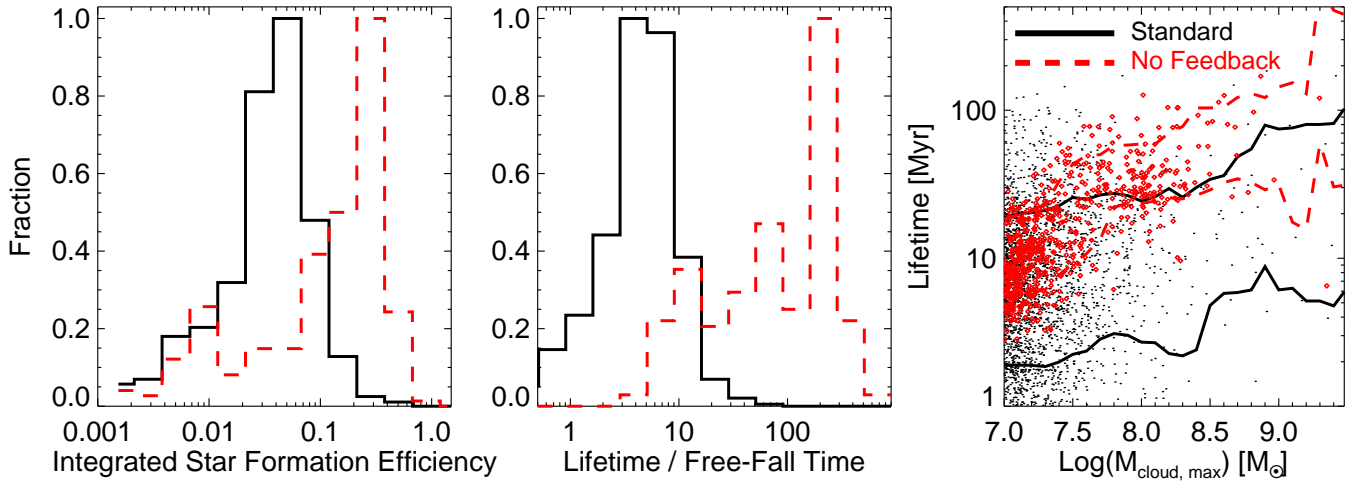


Figure 2. Statistics of gaseous clump lifetimes and star formation efficiencies, in simulations with and without stellar feedback. We identify all gas clumps that can be well-resolved (> 100 particles) down to 10% of the clump mass (> 1000 particles at peak); lifetime is defined as the time above 10% the maximum cloud gas mass. *Left:* Integrated star formation efficiency (stellar mass formed in clump over maximum cloud gas mass). We compare the “standard” model (all feedback included) to a model with no feedback. *Middle:* Cloud lifetime in units of the (mass-weighted average) free-fall time $t_{\text{ff}} \approx 0.54/\sqrt{G\rho}$ within the clump. *Right:* Lifetime versus maximum cloud gas mass. We show the result for individual clouds (small black and large red points for the standard/no feedback models, respectively) and the lines show the $\pm 1\sigma$ range at each cloud mass for each model. With feedback present, even the most massive gas clouds live for a few dynamical times and turn $\sim 10\%$ of their mass into stars. Without feedback, clouds persist until most of their dense gas is turned into stars, giving star formation efficiencies of $\sim 50\%$; their lifetimes are longer and they “end” only because the gas is exhausted (the relic stellar clumps are much longer-lived).

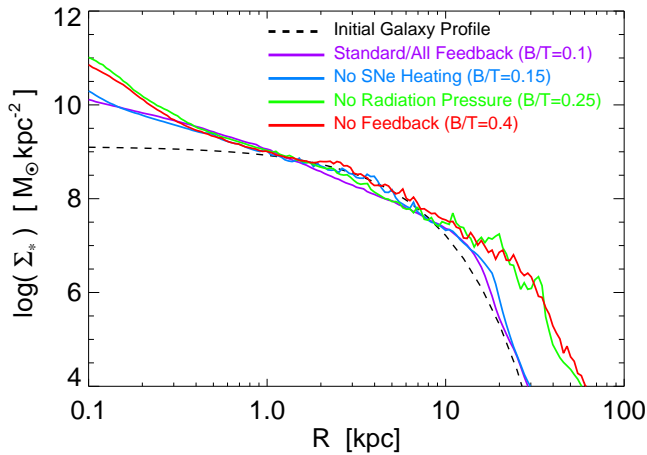


Figure 3. Remnant stellar mass profiles for our simulations, with different stellar feedback mechanisms enabled or disabled (as labeled). The profiles are averaged over ~ 100 projections. The initial disk profile is shown for comparison. There is internal (rapid “secular”) evolution in all cases: gas that loses angular momentum builds a pseudo-bulge while some gas gains angular momentum, making the outer disk larger. With our standard feedback model, the bulge is small ($B/T \sim 0.1$) and disk ($n_s \sim 1$), and the outer disk does not evolve significantly. Removing SNe heating makes little difference. Removing radiation pressure, however, is nearly identical to removing all feedback, which yields a much larger, more concentrated ($n_s \sim 2$) bulge as well as a stellar envelope at large radii that includes $\sim 60 - 70\%$ of the mass.

away from the stellar center. Because this is interior to clouds, the systems are always optically thick, so the latter is approximately $\dot{P}_{\text{rad}} \approx (1 + \tau_{\text{IR}}) L_{\text{incident}}/c$, where $1 + \tau_{\text{IR}} = 1 + \Sigma_{\text{gas}} \kappa_{\text{IR}}$ accounts for the absorption of the initial UV/optical flux and multiple scatterings of the IR flux if the region is optically thick in the IR (with Σ_{gas} calculated for each particle given its location in the clump).

(2) **Supernova Shock-Heating:** Gas shocked by supernovae can be heated to high temperatures. We tabulate the SNe Type-I and Type-II rates from Mannucci et al. (2006) and STARBURST99, respectively, as a function of age and metallicity for all star particles and stochastically determine at each timestep if a SNe occurs. If so, the appropriate mechanical luminosity is injected as thermal energy in the gas within a smoothing length (nearest 32 gas neighbors) of the star particle.

(3) **Gas Recycling and Shock-Heating in Stellar Winds:** Gas mass is returned to the ISM from stellar evolution, at a rate tabulated from SNe and stellar mass loss (integrated fraction ≈ 0.3). The SNe heating is described above. Similarly, stellar winds are assumed to shock locally and inject the appropriate tabulated mechanical luminosity $L(t, Z)$ as a function of age and metallicity into the gas within a smoothing length.

(4) **Photo-Heating of HII Regions:** We also tabulate the rate of production of ionizing photons for each star particle; moving radially outwards from the star, we then ionize each neutral gas particle (using its density and state to determine the necessary photon number) until the photon budget is exhausted. Ionized gas is maintained at a minimum $\sim 10^4$ K until it falls outside an HII region.

(5) **Long-Range Radiation Pressure:** Photons which escape the local GMC (not absorbed in mechanism (1) above) can be absorbed at larger radii. Knowing the intrinsic SED of each star particle, we attenuate integrating the local gas density and gradients to convergence. The resulting “escaped” SED gives a flux that propagates to large distances, and can be treated in the same manner as the gravity tree to give the local net incident flux on a gas particle. The local absorption is then calculated integrating over a frequency-dependent opacity that scales with metallicity, and the radiation pressure force is imparted (and luminosity removed).

In implementing (1)-(5), all energy, mass, and momentum-injection rates are taken from stellar population models (Leitherer et al. 1999), assuming a Kroupa (2002) IMF, without any free pa-

rameters. More details, numerical tests, and resolution studies (up to 10^9 particles with 3.5 pc softening lengths) for these models are discussed in Paper II.

We note that some recent studies of low-resolution cosmological simulations comparing GADGET and the moving mesh code AREPO (Springel 2010) have highlighted some differences between smoothed particle hydrodynamics and grid methods for some cosmological inflow problems (Vogelsberger et al. 2011; Kereš et al. 2012; Torrey et al. 2011). However, we have also performed idealized simulation comparisons between the individual, high-resolution galaxy models here (as well as galaxy mergers) and found excellent agreement for e.g. the star-formation rates, gas inflow through the disk, and surface density profiles; these comparisons will be presented in Hayward et al. (2011). We have also re-run the simulations here with an alternative density-independent formulation of SPH (which resolves these discrepancies) as proposed in Saitoh & Makino (2012); again we find excellent agreement. This owes in part to the resolution, as well as to the fact that the code differences are minimized when flows are super-sonic, always true here (see Bauer & Springel 2012). To the extent that there are differences, the moving-mesh methods may tend to slightly shorter clump lifetimes because stripping and mixing of the gas as it moves are more efficient (and artificial shock dissipation is reduced) (see Sijacki et al. 2012).

3 RESULTS

Fig. 1 compares the gas and stellar⁴ morphologies of runs with varying feedback properties. In all cases, the disks form massive ($> 10^8 M_\odot$) \sim kpc-scale clumps, which in turn form massive star cluster complexes. The gas densities are sufficiently high that extinction can lead to a clumpy optical morphology as well (by entirely extinguishing out regions in the galaxy). The clumpiness is prominent in the gas and stars (although, with feedback present, there is a low surface brightness smooth stellar disk that is not visible at the present observational depth). Seen edge-on, the gas can resemble a “clump-chain” morphology. With feedback present, strong outflows arise from throughout the disk, driven by a massive star formation rate of $> 100 M_\odot \text{ yr}^{-1}$.

In previous papers, we present detailed comparisons between our simulated disk properties and observations. The model disk masses, rotation curves, scale lengths, and gas fractions (see § 2) are chosen to match those observed. Their resulting SFRs ($50 - 300 M_\odot \text{ yr}^{-1}$) are consistent with the Kennicutt-Schmidt relation (Paper I; Fig. 11 and Paper II; Fig. 7). Moreover, the simulated galaxies self-regulate at Toomre $Q \approx 1$, with typical line-of-sight gas velocity dispersions $\sigma \approx 50 - 80 \text{ km s}^{-1}$ and star-forming gas disk scale heights $h \approx 1 \text{ kpc}$ or $h/R \approx 0.2$ (Paper II; Fig. 9). However, we show in Paper II that our model disks always reach $Q \sim 1$ and so – for fixed global disk properties – σ is almost completely independent of the SFR density and the microphysics of feedback. The maximum clump masses are $\sim 10^9 M_\odot$ with a few clumps per disk within a factor of a few of this mass (Paper II; Fig. 13); the

corresponding clump sizes are $\sim 0.3 - 2 \text{ kpc}$ (Paper II; Fig. 15) giving typical clump surface densities $\sim 300 - 1000 M_\odot \text{ pc}^{-2}$ (Paper II; Fig. 14). The clumps are marginally bound (and not rotationally supported, although mildly anisotropic), giving them internal velocity dispersions nearly equal to that of the “background” disk gas (Paper II; Fig. 16; see also Hopkins 2012). The winds driven off of the disk and clumps have a broad velocity distribution from $\sim 200 - 750 \text{ km s}^{-1}$ (Paper III; Fig. 4), with globally averaged outflow rates in the high-speed superwind of $\dot{M}_{\text{wind}} \approx 0.5 - 2 \dot{M}_*$ (Paper III; Figs. 6-7). All of these properties agree reasonably well with those observed (see Genzel et al. 2011, and references therein). As shown in Paper II and Paper III, the simulations quickly establish these properties in the first couple dynamical times and maintain them in quasi-steady state as long as they are evolved, until gas is exhausted.

We now quantify the properties of the clumps in more detail and discuss their implications for the internal (“secular,” but rapid) evolution of the galaxy. We identify gas clumps following Paper II; specifically, we apply the sub-halo finder SUBFIND to the gas, which employs a friends-of-friends linking algorithm with an iterative procedure to robustly identify overdensities (for details and tests, see Springel et al. 2001). In Paper II we show that visual inspection and calculation of the binding energy of clumps confirm that this correctly identifies the obvious clumps; changing linking lengths and other numerical quantities has a weak effect on the properties here. Because the gas particles are unique, we can link clumps in time between different narrowly spaced snapshots ($\Delta t \approx 10^6 \text{ yr}$) to construct a clump “merger tree.”⁵ We then obtain the growth/decay in mass with time for each clump; we define the clump “lifetime” as the time spent above 10% of the maximum clump mass (this cut is arbitrary, but not critical to our results). We can also define the total clump star formation efficiency by integrating the SFR of all clump-associated particles at each time.

Fig. 2 plots the distribution of gas clump lifetimes and star formation efficiencies. As shown in Paper II, the most massive gas clumps do tend to be longer-lived; however, with feedback present their lifetimes are still just a few internal dynamical times ($\sim 10 - 100 \text{ Myr}$; this is consistent with the – highly uncertain – observed stellar populations in clouds in e.g. Elmegreen et al. 2009; Förster Schreiber et al. 2011b, but more detailed observations would present a useful constraint on the predictions here). This is short compared to their inspiral time by dynamical friction. About $\sim 5 - 20\%$ of the peak gas mass of the clumps is turned into stars; this is a factor of a few higher than the star formation efficiency of local GMCs (as expected by theoretical arguments; see Murray et al. 2010), but much less than the order-unity fraction needed to conserve the “relic” stellar clump as a bound entity.⁶

Without feedback, the gas collapses to higher densities rapidly, so the free-fall time $\propto \rho^{-1/2}$ becomes very short and the gas lifetime in units of that free-fall time becomes as long as $\sim 10 - 100 t_{\text{ff}}$. This runaway collapse leads to large star formation efficiencies $\sim 20 - 100\%$, with a mean of $\sim 50\%$ (it is not 100% because there is always some low-density material associated with

⁴ The stellar luminosity in each band is calculated from each star particle according to the STARBURST99 model given its age, mass, and metallicity (and smoothed over the appropriate kernel). We then attenuate the stars following the method of Hopkins et al. (2005): we calculate the total dust column (from the simulated gas) along the line-of-sight to each star particle for the chosen viewing angle (assuming a constant dust-to-metals ratio, i.e. dust-to-gas equal to the MW value times Z/Z_\odot), and apply a MW-like extinction and reddening curve (as tabulated in Pei 1992).

⁵ Here the “main branch” is defined by the most massive clump in the tree at each time. Mergers of other clumps are generally small – most growth is via accretion of “non-clump” gas, so we neglect the “merged branches.”

⁶ Many of the lowest mass-clumps, in both the models with and without feedback, have short lifetimes. The reason is, as shown in Paper II, many of these are never bound but are simply transient overdensities. We also caution that they may still be subject to resolution effects. But in any case these represent a small fraction of the total gas mass and SFR.

clouds). Note that the lifetime of the “gas clump,” defined as we consider it, may then still be relatively short, $\sim 20 - 100$ Myr; this is because most of the mass has turned into stars, a large fraction of which remains self-gravitating and will survive in a bound stellar clump until reaching the galaxy center.

Fig. 3 shows the resulting mass profiles at $t = 500$ Myr (for the initial disk model, $t_{\text{dyn}} \equiv R_e/V_c(R_e) \approx 12$ Myr, so this is 40 (7) dynamical (orbital) times at R_e). By this point the gas is largely exhausted or blown out in all models and the evolution has slowed down; most “sinking” clumps have coalesced. That is not to say this is a “final state” – the system undergoes continuous long-term collisionless stellar/halo internal and secular evolution, and in a cosmological context it would evolve significantly over $\sim \text{Gyr}$ timescales. We are simply comparing the relative effects of including or not including feedback.

In all the simulations, there is some internal/“secular” evolution away from the initial disk conditions. The gas is still asymmetric and turbulent, hence there are gravitational torques (see e.g. Gammie 2001; Hopkins & Quataert 2011; Dekel et al. 2009a; Bournaud et al. 2011; Forbes et al. 2012). Some mass is channeled to the central $\sim \text{kpc}$, building up the “bulge”; the angular momentum loss required for this is absorbed by the outer disk (basically the equivalent of an outer Lindblad resonance), which then migrates outwards into a more extended, flattened disk “envelope” (which may, in some cases, be directly observed; Elmegreen & Elmegreen 2006).

With feedback, this evolution is modest; fitting a bulge-disk decomposition to the profile (with a Sersic-profile bulge and exponential disk), we obtain $(B/T, n_s, R_d) = (0.10, 1.1, 4.3 \text{ kpc})$ for the bulge mass fraction, Sersic index (lower $n_s < 2$ representing more disk-like “pseudobulges”), and disk effective radius (compare to the initial $R_d = 2.7 \text{ kpc}$).⁷ With no feedback, we see a dramatic central rise in the profile indicative of a large bulge, and a much more pronounced outwards evolution of the disk; $(B/T, n_s, R_d) = (0.37, 1.9, 10 \text{ kpc})$. Fig. 3 compares several intermediate cases as well: if we remove radiation pressure, including only sources of gas “heating” (SNe, stellar wind shock-heating, and HII heating), the evolution is only slightly less severe than the feedback-free case. But if we include only radiation pressure, the profile is only somewhat more evolved than the standard feedback case. If, however, we remove long-range radiation pressure forces, keeping only local radiation pressure in regions optically thick in the IR, then it is again more similar to the feedback-free case. As we show in Paper I and Paper III, the long-range photon momentum is critical for driving winds; the short-range pressure tends to drive local turbulence within clumps, but may not completely disperse them.

4 DISCUSSION

We have simulated the isolated internal (rapid secular) evolution of gas-rich (initial $f_{\text{gas}} \approx 0.6$), massive ($10^{11} M_\odot$), disk-dominated

⁷ We caution that the best-fit bulge profile (both with and without feedback) is quite sensitive to the exact fitting procedure, since these galaxies (being clumpy and asymmetric) do not have a well-defined “center” at the sub-kpc level (so it makes a large difference whether we center on a clump density maximum or between clumps). Here we use an iterative elliptical aperture density smoothing to isolate the central density maximum (see Hopkins et al. 2009), which gives the maximum “bulge” component of any fitting methods we explore. Our qualitative conclusions on relative bulge formation efficiencies are the same with each method. The outwards evolution of the disk, however, is a much more robust indication of the degree of internal evolution and is completely insensitive to these fitting details.

galaxies, designed to resemble the most massive star-forming disks observed at redshifts $z \sim 2 - 3$. Our simulations include explicit, physical models for stellar feedback from a variety of sources: radiation pressure (from UV and IR photons), HII photoionization, SNe, and stellar winds. In Paper II, we show that these models agree reasonably well with observed systems in a wide range of measurable properties: effective radius, mass, gas fraction, and rotation curve (by construction), as well as gas velocity dispersion, SFR, Toomre Q parameter, gas disk scale height ($h/R \approx 0.2$), and characteristic clump masses and sizes. Here we have quantified the galaxy morphology and the evolution of its stellar mass profile with different feedback mechanisms included or removed from the simulations.

We find that the models all experience some degree of internal evolution. This is expected: they are all gas-rich, disk-dominated systems in which the cooling time is short relative to the dynamical time, so are both locally and globally gravitationally unstable. We showed in Paper II that, independent of the details of feedback, the disks converge to $Q \sim 1$, which means that the gas velocity dispersion in all cases is essentially identical.⁸ This means that the characteristic Toomre length and mass scales are set by global properties and are similar in all of our simulations, even with very different feedback physics: $M_{\text{Toomre}} \sim h^2 \Sigma_{\text{gas}} \sim f_{\text{gas}}^3 M_{\text{disk}} \sim 10^9 M_\odot$. The size and mass scales for the most massive clumps are therefore similar in all our simulations. In Paper II we explicitly show that the mass function of gas clumps is also broadly similar. These clumps, then, are the generic extension of GMCs in the MW (which has a lower Toomre mass) to more gas-rich massive systems (although with some subtle distinctions; see Krumholz et al. 2012).

However, the effects of the resulting clumps on bulge formation depends strongly on the inclusion of feedback. With no feedback, the clumps collapse rapidly and turn $\sim 50\%$ of their mass into stars. They have no alternative but to sink to the center in a few orbital periods: this gives rise to a massive, $\sim \text{kpc}$ -scale bulge, and causes substantial migration of the remaining disk gas and stars to larger radii (since the angular momentum of the sinking clumps must be taken up by the remaining gas/stars, and tends to do so near the equivalent of an outer Lindblad resonance). These effects are, broadly speaking, well-known results of strong internal/secular evolution, though some of the details differ in this very clumpy limit (and may differ further with ongoing accretion). For an isolated disk, this evolution is self-terminating once sufficient bulge mass is formed, since the outward disk migration and inner bulge formation both stabilize the system; this generically leaves a large low-density disk “envelope” rather than a pure bulge (a well-known result shown in Elmegreen et al. 2005a; Bournaud et al. 2007).

In our standard feedback model – with all mechanisms included – even the most massive clumps tend to be disrupted after they turn $\sim 5 - 20\%$ of their mass into stars. Even if those stars can remain bound after the clump is dispersed (in which case they will still tend to sink to the center, albeit on a factor ~ 10 longer timescale) this suppresses the efficiency of bulge formation via clump coalescence by an order of magnitude. And indeed we see much less dramatic signatures of internal/secular evolution: both a smaller bulge, and much weaker evolution of the outer disk. The re-

⁸ This does not mean the dispersion cannot be “driven by” feedback; it simply means that once systems reach $Q > 1$, excess energy is lost (e.g. in winds) or dissipated, without new star formation, and once $Q < 1$, they collapse until sufficient stars form (or until sufficient gas is exhausted) to bring Q back up to unity.

sulting evolution is less rapid compared to one-way fragmentation, and produces a more traditional pseudobulge. However, the clump morphologies are not radically different; if anything, the clumps appear somewhat *more* prominent with feedback, because they are prevented from internally collapsing to small sizes. They are also less rotationally supported in better agreement with the observations (Förster Schreiber et al. 2011b; Genzel et al. 2011; Swinbank et al. 2011)⁹

A natural prediction of this model is that the old stars should be more smoothly distributed than the gas and young stars (somewhat evident in Fig. 1).¹⁰ A related prediction is plainly that the clumps are relatively short-lived, with gas-phase lifetimes shown in Fig. 2; to some extent this should be manifest as young stellar population ages for the stars physically bound to the clumps. Testing these predictions requires observations that can probe the rest-frame near infrared structure of these galaxies. Moreover, patchy obscuration (given the very large gas densities) can make even the oldest background populations appear clumpy (see Genel et al. 2012). And as also noted in Genel et al. (2012), the fact that clumps form from *both* gas and stars means that – especially if the star formation efficiency is low and lifetimes are short – there will always be contributions to from pre-existing disk stars (with \sim Gyr ages), which will introduce contaminating old stellar populations to all clumps as well as gradients in the clump ages with galactocentric radius (the clump age gradients simply tracing the pre-existing disk gradients). We therefore defer more detailed predictions of clump appearance in different observed wavelengths to future work, in which we will use radiative transfer models to construct mock observations. However, preliminary observational studies have already shown that clumps dominate the light only in young stellar populations and represent transient local fluctuations in luminosity; when constructing stellar mass maps, clumps become far less significant (Wuyts et al. 2012). A rigorous comparison of the simulations here (using mock observations in the relevant observed bands) and these observations will be the subject of future work, but preliminary comparisons suggest that they strongly disfavor the “weak/no feedback” models (Wuyts et al., in prep).

Which feedback mechanisms are most important in dissociating clumps and recycling gas into the ISM? We have shown in Paper II and Paper III that in these dense, gas-rich systems radiation pressure is dominant over sources of thermal heating such as shocked SNe ejecta, stellar winds, and HII photoionization. This is because the gas densities within clumps are so large that the cooling time is significantly shorter than the dynamical time. This explains why previous simulations with feedback included only in the form of thermal heating from SNe have seen very little effect on the evolution of massive star-forming disks (see § 1).

Within the context of radiation pressure, we also find that it is specifically the ability to drive winds out of clumps (and, possibly but not necessarily, the galaxy) that has the largest effect on long-term clump survival and bulge formation. This supports the conclusions of Genel et al. (2012), who found the same in fully cosmological simulations, but with a phenomenological wind model (see § 1). Since the models here self-consistently produce winds with

comparable global mass-loading factors (see Paper III), many of the conclusions should be the same (and we should expect to find similar results in cosmological simulations). In detail, the global wind mass-loading factors here are relatively modest, $\dot{M}_{\text{wind}} \approx \dot{M}_*$ (Fig. 6-7 in Paper III), a factor of ≈ 4 lower than those in Genel et al. (2012) and closer to the values (at this mass and redshift) typically invoked in cosmological models to reproduce the galaxy stellar mass function (Oppenheimer et al. 2010).¹¹ But the implications for clump survival are similar. The reason is that the feedback models here give rise to large *local* outflows and fountains (which do not appear in the Genel et al. 2012 model), driving turbulence and outflows from individual clumps at modest velocities (several tens of km s^{-1}). This is sufficient to unbind gas from a clump but not from the galaxy as a whole. Only a fraction of the material in these fountains is then further accelerated into the galactic outflow at $> 100 \text{ km s}^{-1}$. A generic expectation of our more realistic models is that there should be significantly more mass at modest velocities compared to the true “super-wind;” therefore even modest mass-loading factors of $\gtrsim 0.5 \dot{M}_*$ at high velocities are consistent with our predictions here and probably correspond to sufficient local outflows and fountains to suppress clump inspiral.

Krumholz & Dekel (2010) used analytic models to consider whether or not radiation pressure would disrupt the clumps observed in high redshift galaxies, and concluded that it would not. There are a number of important differences between the full non-linear results here and their simplified model. The clouds here are clumpy and marginally bound, with a large fraction of the clump mass only transiently associated with a given cloud (as opposed to tightly bound or virialized; see Paper II). A combination of disk shear, gravitational instability and feedback operate simultaneously (lowering the threshold for efficient feedback). Krumholz & Dekel (2010) assumed a minimal momentum flux from young stars (about the flux from the single scattering limit); considering the additional contributions from SNe and stellar wind momentum flux, and multiple scatterings in the IR, the momentum flux here is a factor of several larger. And they assumed a star formation efficiency of $\sim 1\%$ per clump dynamical time, even though they argue that this fails to prevent collapse. In Paper I and Paper II, we show that whenever feedback is insufficient to disperse a GMC, runaway local collapse proceeds until the SFR increases to the level needed to once again further suppress collapse (see also Tasker 2011; Dobbs et al. 2011). Thus a higher efficiency always arises when feedback is “initially” insufficient. Overall, our calculations demonstrate that an instantaneous star formation efficiency of just $\sim 1 - 5\%$ (or an integral efficiency of $\sim 5 - 20\%$) is more than sufficient to unbind (most of) the clumps.

Given the stellar feedback mechanisms above, the models here predict local outflows from clumps in qualitative agreement with observations (Genzel et al. 2011; Newman et al. 2012). Both our models here and those in Genel et al. (2012) indicate that, if the wind mass is comparable to that observed, clumps will, in fact, tend to be disrupted. This is also consistent with what is observed at low redshifts (albeit in different galaxy types): in some starburst and mergers the densities and velocity dispersions are similar to these high-redshift systems, and so the characteristic Toomre mass is similar; indeed, ~ 100 GMCs with masses $\sim 10^8 - 3 \times 10^9 M_\odot$ and radii $\sim 0.1 - 1$ kpc have been observed in the local Universe in

⁹ The more prominent rotation – since there is no vertical feedback support – in the no-feedback case leads to the mini-spiral structure seen in some cases in Fig. 1; for a more detailed discussion of the rotation support in the SNe-only case, we refer to Ceverino et al. (2012).

¹⁰ This is always true to some extent, however it will plainly be moreso if the clumps themselves are short-lived and transient, rather than long-lived features.

¹¹ For a detailed comparison of the wind mass-loading, structure, velocities, and phases with observations and cosmological constraints, we refer to Paper III.

such extreme systems (see Rand & Kulkarni 1990; Planesas et al. 1991; Wilson et al. 2003, 2006, and references therein). A combination of constraints from stellar population ages and masses, the maximum mass of star clusters observed in the same galaxies, the specific frequencies of bound/globular clusters, and the cluster formation rates all suggest that these clumps have (gas) lifetimes $\lesssim 100$ Myr, turn only a modest fraction $\sim 10\%$ of their mass into stars, and typically do not remain bound. In future work, we will extend our low-redshift models to starbursts and mergers to compare directly with these observations, but preliminary comparison suggests that they self-regulate in similar fashion.

Our calculations do not include the inflow of gas via continuous accretion and mergers in a cosmological context. This allows us to robustly distinguish the effects of true isolated evolution and disk instability from e.g. ongoing minor mergers. But as a result, our conclusions should be viewed as statements about the relative efficiency of internal evolution with and without feedback, not statements about absolute bulge masses/structure. If the models here are representative of evolution over a few hundred Myr, then a minor merger of mass ratio 10:1 or larger would be able to induce comparable bulge growth, and a major merger would change the system's properties by more than several Gyr of evolution in this mode. Continuous accretion may, however, accelerate the evolution produced by the short-lived clumps and/or effect angular momentum transfer (see Kereš et al. 2005). In future work, we will extend these models to cosmological zoom-in simulations to explore these questions in more detail.

ACKNOWLEDGMENTS

We thank our referee, Avishai Dekel, for a number of insightful comments. We also thank Stijn Wuyts, Reinhard Genzel, Sarah Newman, and Sandy Faber for helpful discussions throughout the development of this manuscript. Support for PFH was provided by NASA through Einstein Postdoctoral Fellowship Award Number PF1-120083 issued by the Chandra X-ray Observatory Center, which is operated by the Smithsonian Astrophysical Observatory for and on behalf of NASA under contract NAS8-03060. EQ is supported in part by the David and Lucile Packard Foundation. NM is supported in part by NSERC and by the Canada Research Chairs program. DK acknowledges support from NASA through Hubble Fellowship grant HSTHF-51276.01-A. The simulations in this paper were run on the Odyssey cluster supported by the FAS Science Division Research Computing Group at Harvard University.

REFERENCES

- Abraham, R. G., Tanvir, N. R., Santiago, B. X., Ellis, R. S., Glazebrook, K., & van den Bergh, S. 1996, *MNRAS*, 279, L47
- Agertz, O., Teyssier, R., & Moore, B. 2009, *MNRAS*, 397, L64
- Barnes, J. E., & Hernquist, L. 1996, *ApJ*, 471, 115
- Barnes, J. E., & Hernquist, L. E. 1991, *ApJL*, 370, L65
- Bauer, A., & Springel, V. 2012, *MNRAS*, 423, 3102
- Bournaud, F., Dekel, A., Teyssier, R., Cacciato, M., Daddi, E., Juneau, S., & Shankar, F. 2011, *ApJL*, 741, L33
- Bournaud, F., Elmegreen, B. G., & Elmegreen, D. M. 2007, *The Astrophysical Journal*, 670, 237
- Bournaud, F., et al. 2008, *A&A*, 486, 741
- Ceverino, D., Dekel, A., & Bournaud, F. 2010, *MNRAS*, 404, 2151
- Ceverino, D., Dekel, A., Mandelker, N., Bournaud, F., Burkert, A., Genzel, R., & Primack, J. 2012, *MNRAS*, 420, 3490
- Chapman, S. C., Blain, A. W., Smail, I., & Ivison, R. J. 2005, *ApJ*, 622, 772
- Cowie, L. L., Hu, E. M., & Songaila, A. 1995, *AJ*, 110, 1576
- Daddi, E., et al. 2010, *ApJ*, 713, 686
- Dekel, A., Sari, R., & Ceverino, D. 2009a, *ApJ*, 703, 785
- Dekel, A., et al. 2009b, *Nature*, 457, 451
- Dobbs, C. L., Burkert, A., & Pringle, J. E. 2011, *MNRAS*, 413, 528
- Elmegreen, B. G., Bournaud, F., & Elmegreen, D. M. 2008, *ApJ*, 688, 67
- Elmegreen, B. G., Elmegreen, D. M., Fernandez, M. X., & Lemoines, J. J. 2009, *ApJ*, 692, 12
- Elmegreen, B. G., Elmegreen, D. M., Vollbach, D. R., Foster, E. R., & Ferguson, T. E. 2005a, *ApJ*, 634, 101
- Elmegreen, D. M., & Elmegreen, B. G. 2006, *ApJ*, 651, 676
- Elmegreen, D. M., Elmegreen, B. G., & Hirst, A. C. 2004a, *ApJL*, 604, L21
- Elmegreen, D. M., Elmegreen, B. G., Rubin, D. S., & Schaffer, M. A. 2005b, *ApJ*, 631, 85
- Elmegreen, D. M., Elmegreen, B. G., & Sheets, C. M. 2004b, *ApJ*, 603, 74
- Evans, N. J., et al. 2009, *ApJS*, 181, 321
- Evans, II, N. J. 1999, *ARA&A*, 37, 311
- Forbes, J., Krumholz, M. R., & Burkert, A. 2012, *ApJ*, 754, 48
- Förster Schreiber, N. M., et al. 2006, *ApJ*, 645, 1062
- . 2011a, *ApJ*, 731, 65
- . 2011b, *ApJ*, 739, 45
- Gammie, C. F. 2001, *ApJ*, 553, 174
- Genel, S., et al. 2012, *ApJ*, 745, 11
- Genzel, R., et al. 2008, *ApJ*, 687, 59
- . 2011, *ApJ*, 733, 101
- Giavalisco, M., Steidel, C. C., & Macchetto, F. D. 1996, *ApJ*, 470, 189
- Governato, F., et al. 2004, *ApJ*, 607, 688
- . 2007, *MNRAS*, 374, 1479
- Greve, T. R., et al. 2005, *MNRAS*, 359, 1165
- Griffiths, R. E., et al. 1994, *ApJL*, 435, L19
- Hammer, F., Flores, H., Puech, M., Yang, Y. B., Athanassoula, E., Rodrigues, M., & Delgado, R. 2009, *A&A*, 507, 1313
- Hayward, C. C., et al. 2011, *MNRAS*, in preparation
- Hernquist, L. 1989, *Nature*, 340, 687
- . 1990, *ApJ*, 356, 359
- Hopkins, P. F. 2012, *MNRAS*, 423, 2016
- Hopkins, P. F., Bundy, K., Croton, D., Hernquist, L., Keres, D., Khochfar, S., Stewart, K., Wetzel, A., & Younger, J. D. 2010, *ApJ*, 715, 202
- Hopkins, P. F., Cox, T. J., Dutta, S. N., Hernquist, L., Kormendy, J., & Lauer, T. R. 2009, *ApJS*, 181, 135
- Hopkins, P. F., & Hernquist, L. 2010, *MNRAS*, 402, 985
- Hopkins, P. F., Hernquist, L., Martini, P., Cox, T. J., Robertson, B., Di Matteo, T., & Springel, V. 2005, *ApJL*, 625, L71
- Hopkins, P. F., & Quataert, E. 2011, *MNRAS*, 415, 1027
- Hopkins, P. F., Quataert, E., & Murray, N. 2011, *MNRAS*, 417, 950
- . 2012a, *MNRAS*, 421, 3522
- . 2012b, *MNRAS*, 421, 3488
- Immeli, A., Samland, M., Westera, P., & Gerhard, O. 2004, *The Astrophysical Journal*, 611, 20
- Kereš, D., Katz, N., Weinberg, D. H., & Davé, R. 2005, *MNRAS*, 363, 2
- Kereš, D., Vogelsberger, M., Sijacki, D., Springel, V., & Hernquist, L. 2012, *MNRAS*, 425, 2027

- Kriek, M., van Dokkum, P. G., Franx, M., Illingworth, G. D., & Magee, D. K. 2009, *ApJL*, 705, L71
- Kroupa, P. 2002, *Science*, 295, 82
- Krumholz, M. R., & Dekel, A. 2010, *MNRAS*, 406, 112
- Krumholz, M. R., Dekel, A., & McKee, C. F. 2012, *ApJ*, 745, 69
- Krumholz, M. R., & Gnedin, N. Y. 2011, *ApJ*, 729, 36
- Krumholz, M. R., & Tan, J. C. 2007, *ApJ*, 654, 304
- Krumholz, M. R., & Thompson, T. A. 2012, *ApJ*, submitted, arXiv:1203.2926
- Kuiper, R., Klahr, H., Beuther, H., & Henning, T. 2012, *A&A*, 537, A122
- Leitherer, C., et al. 1999, *ApJS*, 123, 3
- Mac Low, M.-M., & Klessen, R. S. 2004, *Reviews of Modern Physics*, 76, 125
- Mannucci, F., Della Valle, M., & Panagia, N. 2006, *MNRAS*, 370, 773
- Murray, N., Quataert, E., & Thompson, T. A. 2010, *ApJ*, 709, 191
- Newman, S. F., et al. 2012, *ApJ*, 752, 111
- Noguchi, M. 1999, *ApJ*, 514, 77
- Oppenheimer, B. D., Davé, R., Kereš, D., Fardal, M., Katz, N., Kollmeier, J. A., & Weinberg, D. H. 2010, *MNRAS*, 406, 2325
- Overzier, R. A., et al. 2009, *ApJ*, 706, 203
- . 2010, *ApJ*, 710, 979
- Pei, Y. C. 1992, *ApJ*, 395, 130
- Petty, S. M., de Mello, D. F., Gallagher, J. S., Gardner, J. P., Lotz, J. M., Matt Mountain, C., & Smith, L. J. 2009, *AJ*, 138, 362
- Planesas, P., Scoville, N., & Myers, S. T. 1991, *ApJ*, 369, 364
- Rand, R. J., & Kulkarni, S. R. 1990, *ApJL*, 349, L43
- Robertson, B., Yoshida, N., Springel, V., & Hernquist, L. 2004, *ApJ*, 606, 32
- Robertson, B. E., & Bullock, J. S. 2008, *ApJL*, 685, L27
- Saitoh, T. R., & Makino, J. 2012, *ApJ*, in press, arXiv:1202.4277
- Shapiro, K., et al. 2009, *ApJ*, 701, 955, 11 pages, 6 figures; submitted to *ApJ*
- Shapiro, K. L., et al. 2008, *ApJ*, 682, 231
- Shlosman, I., & Noguchi, M. 1993, *ApJ*, 414, 474
- Sijacki, D., Vogelsberger, M., Keres, D., Springel, V., & Hernquist, L. 2012, *MNRAS*, 424, 2999
- Somerville, R. S., Primack, J. R., & Faber, S. M. 2001, *MNRAS*, 320, 504
- Sommer-Larsen, J., Gelato, S., & Vedel, H. 1999, *ApJ*, 519, 501
- Springel, V. 2005, *MNRAS*, 364, 1105
- Springel, V. 2010, *MNRAS*, 401, 791
- Springel, V., & Hernquist, L. 2003, *MNRAS*, 339, 289
- Springel, V., White, S. D. M., Tormen, G., & Kauffmann, G. 2001, *MNRAS*, 328, 726
- Stewart, K. R., Bullock, J. S., Barton, E. J., & Wechsler, R. H. 2009, *ApJ*, 702, 1005
- Swinbank, A. M., Papadopoulos, P. P., Cox, P., Krips, M., Ivison, R. J., Smail, I., Thomson, A. P., Neri, R., Richard, J., & Ebeling, H. 2011, *ApJ*, 742, 11
- Tacconi, L. J., et al. 2006, *ApJ*, 640, 228
- . 2008, *ApJ*, 680, 246
- . 2010, *Nature*, 463, 781
- Tasker, E. J. 2011, *ApJ*, 730, 11
- Toomre, A. 1964, *ApJ*, 139, 1217
- Torrey, P., Vogelsberger, M., Sijacki, D., Springel, V., & Hernquist, L. 2011, *ApJ*, in press, arXiv:1110.5635
- Vogelsberger, M., Sijacki, D., Keres, D., Springel, V., & Hernquist, L. 2011, *MNRAS*, in press arXiv:1109.1281
- Williams, J. P., & McKee, C. F. 1997, *ApJ*, 476, 166
- Wilson, C. D., Harris, W. E., Longden, R., & Scoville, N. Z. 2006, *ApJ*, 641, 763
- Wilson, C. D., Scoville, N., Madden, S. C., & Charmandaris, V. 2003, *ApJ*, 599, 1049
- Wuyts, S., et al. 2012, *ApJ*, 753, 114
- Zuckerman, B., & Evans, II, N. J. 1974, *ApJL*, 192, L149

APPENDIX A: NUMERICAL EFFECTS OF THE RADIATION PRESSURE IMPLEMENTATION

The numerical details and tests of the feedback models are discussed in great detail in Paper I, Paper II, and Paper III. However, since we argue that radiation pressure is the most important element of feedback in these dense systems, we here discuss how our main conclusions change if we vary numerical aspects of the radiation pressure model implementation.

In Fig. A1, we plot the final mass profiles in the simulations as in Fig. 3, but vary the radiation pressure physics included. The “standard” (all feedback mechanisms included) case and “no radiation pressure” case are the same as Fig. 3.

Recall, the radiation pressure force is coupled in two separate algorithms, the “local IR” and “long-range” terms described in § 2 (mechanisms [1] and [5], respectively). The former includes the effect of primary optical/UV photons absorbed in the immediate vicinity of young stars (within of order a smoothing length), as well as multiple-scattering of the re-emitted IR photons when the IR optical depth τ is significant (which dominate this term when $\tau \gtrsim 1$). The latter includes the effect of the photons escaping this region (UV/optical, and IR) as they propagate to infinity; although the IR term is included, since most of the volume outside the dense regions near stars is optically thin to it, most of the “work” in this term is done by the UV/optical photons being absorbed by less-dense gas further from the dense regions of origin. It is instructive to decompose the effects of these terms.

In the Appendix of Paper II, we discuss at length the accuracy of our long-range radiation pressure approximation. There, we show that although we are not solving the full radiation hydrodynamic equations, the simplifications used here are a surprisingly good approximation to full radiative transfer solutions. Nevertheless, it is important to check how big an effect this has. In Fig. A1, we therefore re-run our simulation, but instead of using the on-the-fly simulation information on stellar populations and gas distributions to calculate the spectral shape escaping and propagating in the long-range radiation pressure term, we simply fix the SED shape to one chosen to match observations. The details of this procedure are given in the Appendix of Paper II; as noted there, choosing instead a mean SED matched to a full radiative transfer calculation on the simulations gives an almost identical result (since it closely matches what is observed). This has almost no effect on our conclusions relative to our “standard” model.

If we remove the long-range terms (mechanism [5] in § 2) entirely, but still include the local/IR term (mechanism [1]), we see a much more significant difference. Both the bulge mass and internal evolution of the outer disk are significantly enhanced above the “standard” model. Most of the new bulge mass is at ~ 1 kpc. The very central regions at $\lesssim 100$ pc are regulated by the IR term and so are still maintained at low densities, but the overall ability to disrupt the \sim kpc-scale clump complexes is reduced. The net effect is comparable to – although still clearly less dramatic than – the effects of removing radiation pressure entirely.

It therefore seems that the long-range radiation acceleration is

at least comparable, if not more important, to the local IR radiation pressure in suppressing the clump star formation efficiencies and subsequent bulge growth. This is true for several reasons: but the critical point is that the kpc-scale complexes have clear substructure. As shown in Paper II, at any given instant, most of the mass in complexes is not in the extremely dense sub-regions forming stars, and this “intermediate-density” material is essentially *never* tightly bound or virialized inside a cloud when feedback is present. The IR radiation pressure, obviously, acts significantly only where the IR opacities are substantial. The volume-average surface densities of the complexes are only marginally optically thick to the IR ($\tau_{\text{IR}} \sim 1$ for $\Sigma_{\text{gas}} \sim 10^9 M_{\odot} \text{ kpc}^{-2}$); so the IR coupling is negligible in the lower-density volume-filling medium inside each complex. The IR coupling is therefore dominated (as shown in Paper I) by very dense sub-clumps at ~ 1 pc scales (densities $\Sigma_{\text{gas}} \gg 10^4 M_{\odot} \text{ kpc}^{-2}$ and three-dimensional densities $n \gtrsim 10^5 \text{ cm}^{-3}$), over a very short time when they have just formed young stars. But these dense sub-regions are distributed throughout the complex, so the IR term does not act *coherently* across the entire cloud complex to disrupt it. Rather, it disrupts the dense star-forming sub-regions shortly after they form stars, recycling the dense gas into the parent complex, at turbulent velocities of order the local escape velocity from the sub-clump ($\sim 10 - 50 \text{ km s}^{-1}$). This makes it optically thin to the IR photons, but (being marginally bound) much more vulnerable to continuous, *coherent* acceleration from the collective UV/optical flux of the all the stars in the complex.

The short-range radiation pressure mechanism – in particular the multiple-scattering of IR photons producing a local momentum flux of $\sim \tau L/c$ – can, in principle, be more affected by the details of accurate radiation transport. For example, Krumholz & Thompson (2012) argue that, in a time-averaged sense, the “boost factor” τ_e in $\dot{p} \sim \tau_e L/c$ does not scale linearly with the full average optical depth τ when $\tau \gg 1$ and does not typically exceed a factor of several. We should stress, however, that our conclusions are actually not that different from those of Krumholz & Thompson (2012). Those authors argue specifically that the reason τ_e is “capped” is because, whenever the radiation pressure force temporarily exceeds gravity, gas is locally blown away and dense regions are “shredded” by radiation Rayleigh-Taylor instabilities, until the coupling is lowered such that radiation balances gravity. Even though we do not follow the full radiation transport, this is the generic behavior in our simulations as well (IR radiation pressure drives to lower effective τ_e to offset gravity). As a result, as discussed in Paper I and Paper II, the IR term primarily drives local turbulence, disrupting or shredding dense sub-regions and driving turbulence to maintain a Toomre $Q \approx 1$, while the long-range radiation pressure (which operates via single scattering and is not affected by this argument) drives winds in loosely-bound material, primarily coupling via its UV/optical opacity. Consider, for example, in Paper I, we show that the mean true IR τ in the dense protostellar core-like regions that have just formed new stars – which dominate the momentum input – can reach as high as $\sim 10 - 50$. However, we also show that the coupling of $\tau L/c$ in these regions immediately (often in < 1 Myr) disperses the gas to lower τ around the source and allows resolved leakage, so that the *luminosity-averaged* coupling factor, i.e. the true τ_e we should compare to Krumholz & Thompson (2012), is actually just $\tau_e \approx 4 - 5$ in our simulations. Both this and the resulting local velocity dispersions and Eddington ratios are in reasonable agreement with these and other radiative transfer calculations (Kuiper et al. 2012, Jonsson et al. in preparation).

Still, one could imagine sub-resolution scale effects that might reduce this local IR coupling. We discuss this extensively in Pa-

per I (Appendix B), and in particular consider the case of a fractal ISM continuing to infinitely small scales below the resolved region used to calculate τ ; as opposed to a homogenous medium, this will present “holes” or “channels” along which photons can leak out. For a lognormal or power-law density distribution, we show that in this particular case it is straightforward to analytically calculate the “effective” coupling and leakage effects. In all cases where τ is large, this dramatically enhances the escape fraction of UV and optical photons. However, if the scatter in density contributed strictly below the resolution scale of $\sim 1 - 10$ pc is weak or modest, $\lesssim 0.5$ dex, then this has no effect on the dimensional scaling of the momentum imparted by multiply-scattered IR photons (rather it just amounts to a weak normalization correction). For larger scatter it introduces a scaling $\tau_e \sim \tau^{\beta}$ where $\beta < 1$ is a weakly decreasing power of the sub-resolution density dispersion. In Paper I we show how this can be implemented in the simulations and used to allow both for the corrected IR coupling and UV/optical escape fractions. We therefore consider two examples using this “leakage” estimator. In the first, we follow Paper I (model “PL: σ calculated” therein) and use the local (resolved) density dispersion added in quadrature with a large assumed floor of ~ 1 dex and the solution for a fractal medium – this results in a highly sub-linear $\tau_e(\tau)$ (approximately $\propto \tau^{1/3}$), and actually produces significantly weaker τ_e values than those calculated in full radiative transfer calculations by either Krumholz & Thompson (2012) or Kuiper et al. (2012). But we see little difference between this and our standard model – if anything, the bulge is slightly smaller! This occurs because, as discussed above, the single-scattering is critical to actually dispersing the cloud complexes, while the IR largely drives local turbulence and is always driven to approximate equilibrium with gravity. The latter equilibration still occurs, even if the coupling is made weaker (gas collapses to slightly higher densities first, giving higher τ to obtain the same τ_e); this is shown explicitly (along with the lack of strong effects on any of our predicted galaxy properties) in Paper I (Figs. 5, 9, 10, B2). And allowing for leakage of course makes the long-range radiation pressure forces *stronger*, by removing fewer of the UV/optical photons in the dense regions near stars where they act less efficiently.

To clearly distinguish between the effects of decreasing the local IR radiation force and increasing the long-range force, we can artificially multiply the local IR radiation pressure by an arbitrary factor, without increasing the UV/optical leakage. Fig. A1 shows such an experiment, with a reduction of the local IR force by a factor of 3, which leads to a very modest galaxy-averaged $\tau_e \approx 2$. As Fig. A1 shows, here we do find more bulge growth and longer-lived clouds than in the previous case, as expected, although the effect is small.

Other effects discussed in Paper I, however, could mean that our implementation actually under-estimates the strength of the radiation pressure terms. For example, if the gas density profiles rise sufficiently steeply around young stars, or if we are under-resolving the maximum densities (hence opacities) to which regions surrounding very young stars collapse, then our simulation-calculated momentum flux could be a substantial under-estimate. Kuiper et al. (2012) also argue that calculations such as Krumholz & Thompson (2012), which do not follow the exact radiative transfer but adopt a pure flux limited diffusion approximation and see efficient dispersal as described above, can underestimate the true coupling efficiency by an order-of-magnitude. Unsurprisingly, we see further reduction of bulge growth and internal evolution in experiments where we enhance the radiation pressure strength to match these suggestions.

Finally, as shown in Paper I and Paper II, we have run reso-

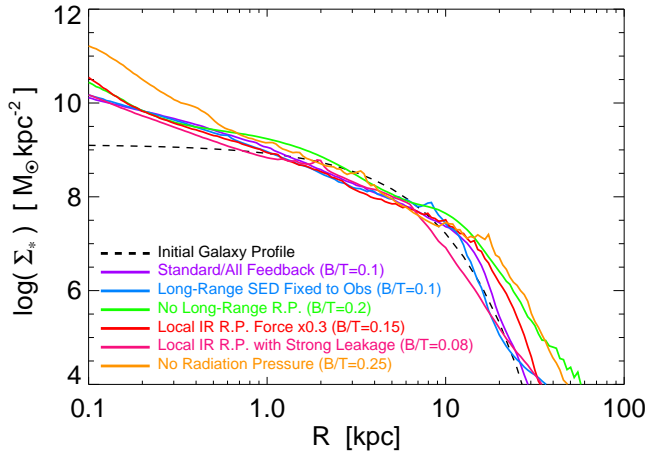


Figure A1. Remnant stellar mass profiles as Fig. 3; here we specifically compare models where we freely vary sub-elements of the radiation pressure implementation. The “standard/all feedback” model and “no radiation pressure model” are identical to Fig. 3. The “long-range SED fixed to obs.” model fixes the spectral shape of the propagated long-range radiation pressure (RP) terms (mechanism [5] in § 2) to the mean observed in the galaxies modeled. This has little effect, since the self-consistently calculated SEDs agree well with the observations. The “no long-range RP” model removes the long-range terms entirely. This significantly suppresses the mixing and disruption of the largest super-clump complexes, resulting in more bulge growth and internal evolution. The “local IR RP force x0.3” model suppresses the local IR RP term (mechanism [1] in § 2) by an arbitrary factor = 0.3. This leads to less feedback-regulation in the dense gas and greater bulge growth, but the effect is weak when the long-range RP is still present. The “local IR RP with strong leakage” model calculates the local IR RP term assuming a sub-grid fractal ISM with a broad density PDF giving a much larger UV/optical escape fraction and weaker multiple-scattering “boost” for a given average dust optical depth in the region. Although this makes the local RP term weaker, the enhanced escape of UV/optical photons from the very dense regions around young stars makes the long-range RP forces significantly stronger and increases the coherent acceleration of gas between the dense sub-cloud cores in the massive cloud complexes (as well as the launching of RP-driven winds); as a result this slightly suppresses the internal evolution relative to the standard model.

lution tests with these models up to $\sim 10^9$ particles and find very good convergence at the standard resolution adopted here; in fact for the bulk properties here we see reasonable convergence even at order-of-magnitude lower particle numbers.